Simulation and Experimental Study of Beam Dynamics in NovoFEL RF Gun and its Beamline

Anton Matveev,[1, 2, a)] Igor Davidyuk,[1] Oleg Shevchenko,[1] Vladimir Tcheskidov,[1] Nikolay Vinokurov,[1, 2] and Vladimir Volkov[1]

[1)]*Budker INP SB RAS, 630090, pr. Akad. Lavrent'eva 11, Novosibirsk, Russia*
[2)]*Novosibirsk State University, 630090, ul. Pirogova 1, Novosibirsk, Russia*

[a)]*Corresponding author: matveev.a.s@yandex.ru*

Abstract. A new normal-conducting, CW, thermocathode RF gun has been developed and tested recently at Budker Institute of Nuclear Physics. Providing an average current of up to 100 mA, this device will be used to upgrade the injector of the Novosibirsk FEL facility. Simulation of beam dynamics in the RF gun and its beamline was performed, the space-charge forces taken into account. Comparison of the simulation results and experimental measurements is presented in this paper.

INTRODUCTION

A new normal-conducting, CW, thermocathode RF gun has been developed and tested recently at Budker Institute of Nuclear Physics [1]. This gun is planned to increase the maximum value of the average electron beam current in the energy recovery linac (ERL) of the Novosibirsk free electron laser (FEL) [2] up to 100 mA as compared with the 30 mA maximum average current from the operating static electron gun. The RF gun will be connected with the injector of the FEL by a beamline containing a 90° bend, which enables two options of operation: using the static or the RF electron gun [3]. The condition of such high current electron beam requires accurate simulations of future magnetic optics regimes of the injector in order to prevent heating of the vacuum chamber walls because of beam losses and, consequently, possible vacuum breakdown. Large bunch charge and low energy lead to strong space-charge forces, which should be taken into account.

We used the ASTRA program package [4] and CST Studio [5] to simulate the beam dynamics in the RF gun and its beamline. The RF gun is now on the test stand (see Fig. 1) for test before installing it in the injector, measurement of the electron beam parameters (which are also used as initial conditions at our simulations), and verification of the simulation model.

In this paper, we present the layout of the RF test stand, description of the simulation model, and comparison of the measurements with respective calculations.

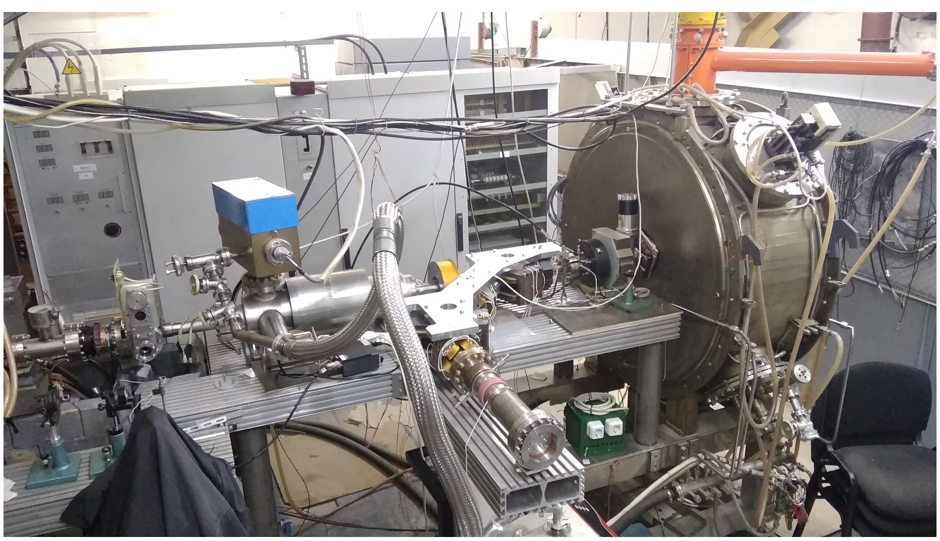

FIGURE 1. View of RF gun test stand with 90° bend fully assembled.

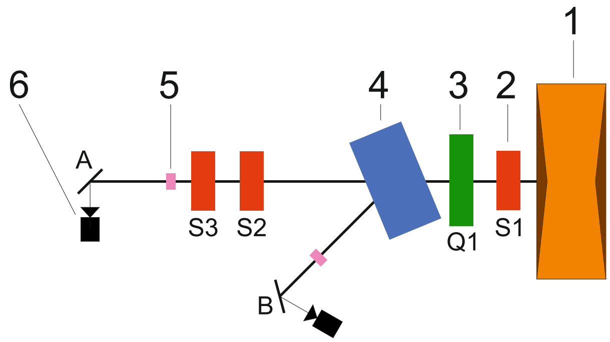

FIGURE 2. Layout of RF gun stand.

GUN DESCRIPTION AND TEST STAND LAYOUT

The main RF gun parameters are listed in Table I. It can produce electron beams with an energy of 300 keV and charge of up to 2 nC at an average current of up to 100 mA. The RF gun uses the same cathode-grid assembly, extracted from the commercially available metalloceramic triode GS-34, as in the static electron gun operating now. The higher average beam current for the RF gun is achieved due to the higher beam repetition rate, which can be varied in the range of 2 kHz – 90.2 MHz. For a more detailed description of the RF gun the reader is referred to [1].

Figure 2 shows the scheme of the RF test stand that was used during the measurements presented at this paper. The electron beam produced and accelerated in RF gun (1) propagates through focusing solenoid (2) and quadrupole lens (3). Then, if dipole magnet (4) is turned off, the beam goes straight through two focusing solenoids and falls on a conductive target. Optical transition radiation (OTR) from the target is observed using CCD video camera (6). Another target for OTR diagnostics is located at the end of the section turned 45° with respect to the straight one. There are two ceramic insulators (5) installed as shown in Fig. 2, which enables us to measure the average beam current falling on the target. The energy of the beam is determined by the accelerating voltage of the RF gun. The dependence of the beam energy on the accelerating voltage was once measured from the time of flight between two resistive beam sensors installed in the straight section [1].

SIMULATIONS

Calculations of beam dynamics in the RF gun and its beamline were made using the ASTRA program package [4] and CST Studio [5] with particle tracking carried out from the cathode surface. It allows simulating a longitudinal beam profile. The grid aperture and cathode-grid electromagnetic fields calculated in a field solver were specified.

In our simulations, we set uniform emission of a round beam with a radius of 6 mm (the radius of the cathode surface) and duration of 2 ns. The cathode-grid voltage cuts out a beam of a duration of around 1 ns, which is then

TABLE I. Main parameters of RF gun

Parameter	Value	Unit
Beam average current	≤ 100	mA
Electron energy	100–300	keV
Bunch charge	≤ 2.0	nC
Bunch length (FWHM)	1.0	ns
Peak current	15	A
Beam repetition rate	0.002–90.2	MHz
RF generator power	≤ 50	kW
Emittance of bunches[a]	≈ 10	mm$\times$mrad

[a] Calculated in ASTRA simulations

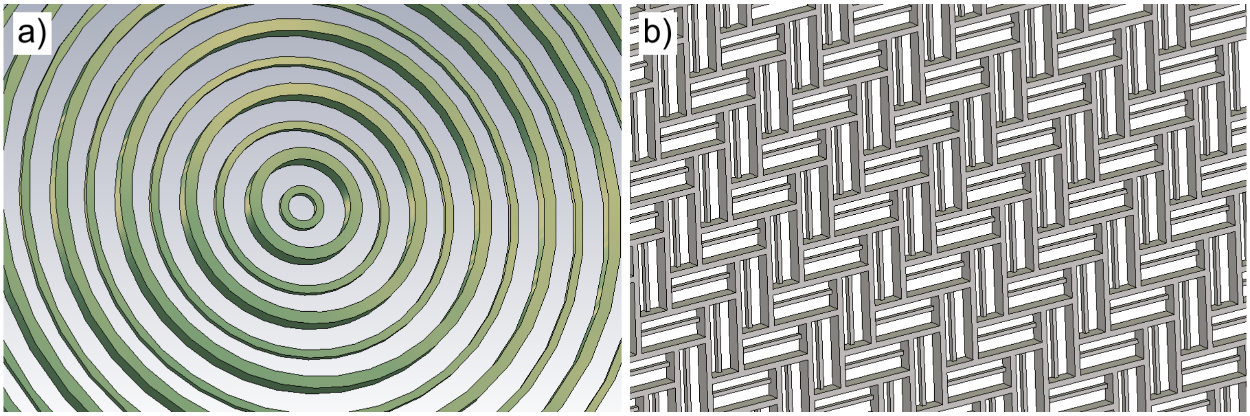

FIGURE 3. Two cathode grid geometries: (a) used in ASTRA simulations; (b) real shape used in CST simulations.

compressed if accelerated in the phase that provides velocity bunching. Initially, only ASTRA was used, in which both the cathode-grid field and the main acceleration one were specified. But it allowed setting only axial symmetric apertures. So, instead of the real grid geometry shown in Fig. 3(b), the grid shape illustrated in Fig. 3(a) was specified. The following equivalence criteria were used: equal geometry transparencies, equal electric field transparencies ($E_{cathode-grid}/E_{grid-anode}$), and equal emittances in the static field for both grid geometries [6]. However, these measures lead to appearance of singularity at the center of the transverse beam profile at the output of the RF gun, as shown in Fig. 4. It results from the existence of the only radial component of electrostatic focusing by the "axial" grid ($1/f \propto \Delta E_z$) [7], which leads to only radial component of the transverse velocity.

To obtain a beam profile distribution close to the Gaussian one, which is observed in measurements, we decided to use the Particle Tracking Solver of CST Studio to simulate the dynamics of electron beam emitted from the cathode and passing through the grid. CST Studio allows specifying the grid with the real geometry shown in Fig. 3(b). However, this solver simulates an electron beam as individual trajectory lines; so, longitudinal motion is not considered. The output of the CST simulation is used as input data for ASTRA tracking of the electron beam in the main accelerating fields of the RF gun and the beamline magnet optics. This technique has resulted in a near-Gaussian beam profile (see Fig. 4). On the one hand, the singularity stated above has been eliminated, and, on the other hand, the longitudinal beam profile must be specified manually as input for further calculations with ASTRA.

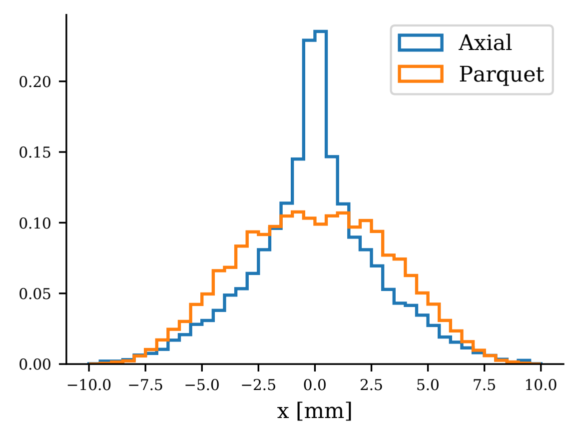

FIGURE 4. Transverse beam profile distribution at output of RF gun with "axial" and "parquet" grid geometry.

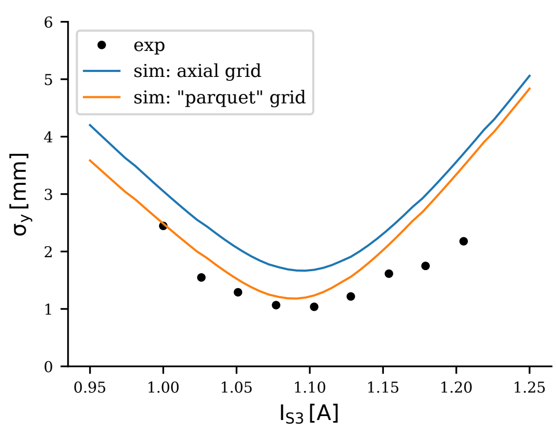

FIGURE 5. Comparison of measured rms beam vertical sizes on OTR monitor A with simulations with "axial" and "parquet" grid geometry.

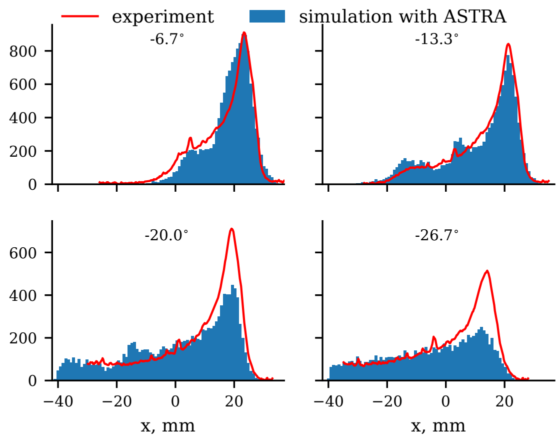

FIGURE 6. Horizontal beam profile distributions and corresponding calculations at different values of RF gun accelerating phases, where 0° is phase of maximum beam acceleration.

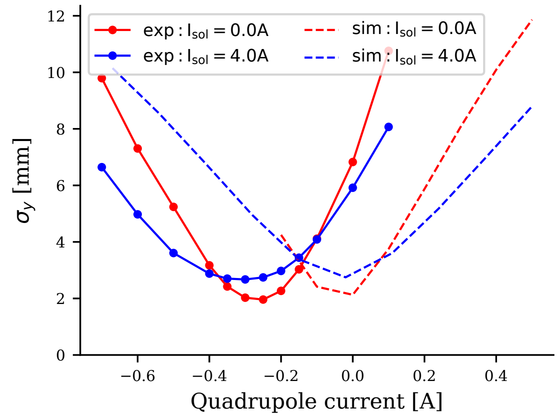

FIGURE 7. Comparison of measured rms beam vertical sizes while varying quadrupole current Q1 with corresponding simulations.

MEASUREMENTS

There are two OTR monitors on the RF gun test stand, referred to as A and B, as shown in Fig. 2, which are installed at the end of the straight and side sections, respectively. CCD cameras are used to register the OTR radiation from these monitors. By varying the beam repetition rate, the cameras were checked for encoding the value proportional to the intensity, i.e., there is no gamma correction ($\gamma = 1$).

Measurements on OTR monitor A

The rms beam vertical sizes on the OTR monitor A were measured while varying the solenoid S3 current. Comparison of the experimental data with respective simulations with "axial" and "parquet" grid geometries is illustrated in Fig. 5. As expected, simulations for the "parquet" grid with a near-Gaussian beam transverse profile give better agreement with the experimental data. The calculated transverse beam emittance is around 16 mm×mrad when the beam size is minimal. The solenoid scan technique for measurements of transverse beam emittance [8] is inapplicable because of strong space charge effects.

Measurements on OTR monitor B

The bend magnet in the stand scheme (Fig. 2) allows measuring the horizontal beam profile on OTR monitor B, corresponding to the energy distribution of the beam from the RF gun. The experiment was conducted in the following way: solenoid S1 was turned off and the quadrupole Q1 strength was chosen such that the horizontal beta function was minimal. Thus, the best energy resolution was achieved:

$$\frac{\delta p}{p_0} \approx \frac{\sqrt{\varepsilon_x \beta_x}}{\eta}$$

where p_0 and δp are the average electron momentum and its rms deviation, respectively, ε_x is the horizontal emittance, and η and β_x are the dispersion and horizontal beta functions at OTR monitor B. The result of the measurements and respective simulations with ASTRA are illustrated in Fig. 6. The scale of the experimental curve was normalized so that the maximum values of the experimental and calculation data were equal when the phase was $-6.7°$. There is good agreement for a phase close to 0°, the phase of maximum beam acceleration. The deviation for RF phases of $-20.0°$ and $-26.7°$ is to study. It may be a result of incorrect duration of beam in the calculations, which could lead to wrong beam energy spread.

The quadrupole scan was used to verify the calculation of beam dynamics in the bend. Figure 7 demonstrates the result of measurements of the rms beam vertical size and respective calculations. There is mismatch between the experimental curves (for solenoid S1 currents of 0.0 A and 4.0 A) and the calculated ones, which can be eliminated by translation of the experimental curves by around -0.2 A along the abscissa. This shift corresponds to the lack of vertical focusing in the simulations, estimated as an additional lens with $f_y \approx 50\,\mathrm{cm}$. The vertical normalized emittances in the simulations are 18.5 and 16.0 mm$\times$mrad for solenoid S1 current of 0.0 and 4.0 A, respectively.

CONCLUSION

Measurements of transverse beam profile and beam energy spread have been performed and presented in this paper. A brief description of the RF gun parameters and the test stand is given. The simulation model is discussed. Now the 90° bend with OTR monitor at the end is being assembled; so, we plan to carry out additional measurements. Besides, measurements of longitudinal beam profile are planned.

REFERENCES

1. V. Volkov, Y. Getmanov, E. Kenjebulatov, E. Kolobanov, S. Krutikhin, G. Kurkin, V. Ovchar, V. Petrov, and I. Sedlyarov, "Thermocathode radio-frequency gun for the Budker institute of nuclear physics free-electron laser," Physics of Particles and Nuclei Letters **13**, 796–799 (2016).
2. O. Shevchenko, V. Arbuzov, N. Vinokurov, P. Vobly, V. Volkov, Y. V. Getmanov, I. Davidyuk, O. Deychuly, E. Dementyev, B. Dovzhenko, *et al.*, "Novosibirsk free electron laser: recent achievements and future prospects," Radiophysics and Quantum Electronics **59**, 605–612 (2017).
3. A. Matveev, I. Davidyuk, O. Shevchenko, V. Tcheskidov, N. Vinokurov, and V. Volkov, "Simulation and optimization of the transport beamline for the NovoFEL RF gun," in *39th Free Electron Laser Conf.(FEL'19)* (JACOW Publishing, Geneva, Switzerland, 2019) pp. 647–650.
4. K. Floettmann, *ASTRA: A Space Charge Tracking Algorithm*, DESY (2017), `https://www.desy.de/~mpyflo/`.
5. *CST Studio*, see `https://www.3ds.com/products-services/simulia/products/cst-studio-suite/`.
6. V. Volkov, E. Kenjebulatov, S. Krutikhin, G. Kurkin, V. Petrov, E. Rotov, and N. Vinokurov, "Thermionic cathode-grid assembly simulations for RF guns," in *23rd Particle Accelerator Conf. (PAC'09)* (JACOW Publishing, Geneva, Switzerland, 2009) pp. 572–574.
7. H. Wiedemann, "Particle accelerator physics," (Springer-Verlag Berlin Heidelberg, 2007) Section 3.7.2, pp. 105–106, 3rd ed.
8. M. Minty and F. Zimmermann, "Measurement and control of charged particle beams," (Springer Nature, 2003) Chap. 4, pp. 101–104.